MATHEMATICAL MODELING AND COMPUTING, Vol. 12, No. 2, pp. 640–649 (2025)

Stability analysis of three-dimensional stagnation-point flow and heat transfer over a permeable stretching/shrinking sheet with heat source effect in viscous fluid

Kamal F.[1,*], Zaimi K.[1,2], Hamid R. A.[1], Bakar N. A. A.[1], Saidin N. A.[1], Halim A. A. A.[3]

[1] *Institute of Engineering Mathematics, University Malaysia Perlis, Pauh Putra Campus, 02600 Arau, Perlis, Malaysia*
[2] *Centre of Excellence for Social Innovation and Sustainability (CoESIS), University Malaysia Perlis, Pauh Putra Campus, 02600 Arau, Perlis, Malaysia*
[3] *Faculty of Electronic Engineering Technology (FTKEN), University Malaysia Perlis, Pauh Putra Campus, 02600 Arau, Perlis, Malaysia*
[*] *Corresponding author: fatinnabila@unimap.edu.my*

(Received 10 January 2025; Revised 19 June 2025; Accepted 21 June 2025)

This study presents the steady three-dimensional stagnation-point flow towards a permeable stretching/shrinking sheet in the presence of heat source effects. The governing equations in the form of partial differential equations are transformed into a system of ordinary differential equations by using similarity transformation, and then solved numerically using bvp4c function in Matlab software. The variations of the numerical solutions for the skin friction coefficient and the local Nusselt number as well as velocity and temperature profiles are obtained for several values of the governing parameters. It is found that the dual solutions exist for the stretching/shrinking case. Stability analysis is performed to determine which solution is stable and physically reliable. Results from the stability analysis show that the first solution is stable while the second solution is not.

Keywords: *three-dimensional flow; stagnation-point; suction/injection effect; heat source effect; stretching/shrinking sheet; stability analysis.*

2010 MSC: 80A20, 76D05, 76N20 **DOI:** 10.23939/mmc2025.02.640

1. Introduction

Recently, the studies of stagnation-point flow has attracted the interest of many researchers due to its applications in industry such as flows over the tips of aircraft and submarines. Hiemenz [1] was the first who study the problem two-dimensional stagnation-point flow against a stationary semi-infinite wall. The problem of three-dimensional stagnation-point flow and heat transfer has importance applications in many manufacturing processes in petrochemical industries, the aerodynamic of plastic sheet, and others [2]. Kumar et al. [3] have studied the magnetohydrodynamic effects on the transient three-dimensional stagnation-point flow of a Casson fluid along a bi-directional stretching sheet. Wahid et al. [4] have considered the numerical and statistical analyses of three-dimensional non-axisymmetric Homann's stagnation-point flow of nanofluids over a shrinking surface. Shafie et al. [5] have investigated the quadratic convective nanofluid flow at a three-dimensional stagnation-point with the g-Jitter effect. Hafidzuddin et al. [6] have studied the effects of ansotropic slip on three-dimensional stagnation-point flow past a permeable moving surface. Since then, many researchers have been working on the stagnation-point effect with various physical conditions such as Jamaludin et al. [7], Rehman et al. [8], Al-Balushi et al. [9], Amirsom et al. [10], Bariş and Dokuz [11], Mohaghegh and Rahimi [12], and Rehman et al. [13].

The study of heat source/sink effect also has attracted many researchers. Recently, Raju and Sandeep [14] considered the effect of heat source/sink on unsteady three-dimensional flow of Casson–Carreau fluids past a stretching surface. Hayat et al. [15] studied the three-dimensional flow of Jeffrey flow over a bidirectional stretching surface with heat source/sink effect. Hayat and Alsaedi [16] explored

the Soret and Dufour effects on three-dimensional flow over an exponentially stretching surface with porous medium, chemical reaction and heat source/sink effects. Kar et al. [17] examined the three-dimensional free convection MHD flow in a vertical channel through a porous medium with heat source and chemical reaction.

Motivated by the aforementioned works, this study aims to analyze the steady three-dimensional stagnation-point flow and heat transfer towards a permeable stretching/shrinking sheet with heat source effect. In the present study, we extend the work of Hafidzuddin et al. [18]. This study is different from that investigated by Hafidzuddin et al. [18], where we consider the stagnation-point and heat source effects. The governing partial differential equations are converted into ordinary differential equations by similarity transformations, before being solved numerically using the bvp4c function in Matlab software. The results on suction/injection and heat source effects are explored and discussed in detail. The dual solutions are expected to exist for both stretching/shrinking case. A stability analysis is conducted to verify which solution is stable and physically reliable.

2. Mathematical formulation

The steady three-dimensional stagnation-point flow of a viscous fluid over a stretching/shrinking sheet with suction/injection and heat source effect is considered. The physical model and coordinate system of the model are given as shown in Figure 1, where x and y are the coordinates of the stretching/shrinking sheet, while the coordinate z is measured in the perpendicular direction to the surface.

It is assumed that the velocity of stretching/shrinking sheet is $u_w(x) = \varepsilon_1\, a\, x$ in x-direction and $v_w(y) = \varepsilon_2\, a\, y$ in y-direction, respectively, where ε_1 and ε_2 are the stretching/shrinking parameters by $\varepsilon_1, \varepsilon_2 > 0$ is the stretching sheet and $\varepsilon_1, \varepsilon_2 < 0$ is the shrinking sheet, respectively along a as positive constants. It is also assumed, that the mass flux velocity is $w = w_e$, where $w_e < 0$ is for suction and $w_e > 0$ is for injection. The velocities of the external flow are $u_e(x) = a\, x$ and $v_e(y) = a\, y$. Under these assumptions, the boundary layer equations are (see Hafidzuddin et al. [18])

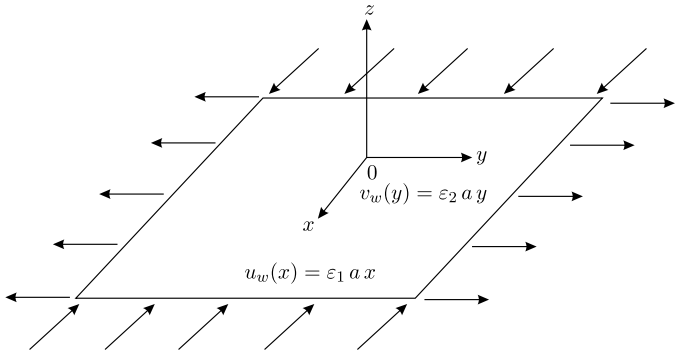

Fig. 1. Physical model and coordinate system for the proposed problem.

$$\frac{\partial u}{\partial x} + \frac{\partial v}{\partial y} + \frac{\partial w}{\partial z} = 0, \tag{1}$$

$$u\frac{\partial u}{\partial x} + v\frac{\partial u}{\partial y} + w\frac{\partial u}{\partial z} = u_e\frac{du_e}{\partial x} + \nu\frac{\partial^2 u}{\partial z^2}, \tag{2}$$

$$u\frac{\partial v}{\partial x} + v\frac{\partial v}{\partial y} + w\frac{\partial v}{\partial z} = v_e\frac{dv_e}{\partial y} + \nu\frac{\partial^2 v}{\partial z^2}, \tag{3}$$

$$u\frac{\partial w}{\partial x} + v\frac{\partial w}{\partial y} + w\frac{\partial w}{\partial z} = w_e\frac{dw_e}{\partial z} + \frac{\sigma B^2}{\rho}(w_e - w) + \nu\frac{\partial^2 w}{\partial z^2}, \tag{4}$$

$$u\frac{\partial T}{\partial x} + v\frac{\partial T}{\partial y} + w\frac{\partial T}{\partial z} = \alpha\frac{\partial^2 T}{\partial z^2} + \frac{Q_0}{\rho C_p}(T - T_\infty) \tag{5}$$

corresponding to the boundary conditions

$$\begin{aligned} &u = u_w(x) = \varepsilon_1 U_w, \quad v = v_w(y) = \varepsilon_2 V_w, \quad w = w_w, \quad T = T_w \quad \text{at} \quad z = 0, \\ &u \to u_e(x), \quad v \to v_e(y), \quad w \to 0, \quad T \to T_w \quad \text{as} \quad T \to \infty, \end{aligned} \tag{6}$$

where u, v and w are velocity components corresponding to the along x-, y- and z-axes, respectively, T denotes the fluid temperature, T_w is the constant surface temperature, ν denotes the kinematic

viscosity, α denotes the thermal diffusivity of the fluid, C_p denotes the specific heat capacity at constant pressure, Q_0 denotes the temperature dependent heat source/sink coefficient and ρ denotes the density of a fluid. Further, the similarity variables are introduced as follows:

$$u = a\,x\,f'(\eta), \quad v = a\,y\,g'(\eta), \quad w = -(a\,\nu)^{\frac{1}{2}s}, \quad \theta(\eta) = \frac{T - T_\infty}{T_w - T_\infty}, \quad \eta = \left(\frac{a}{\nu}\right)^{\frac{1}{2}} z, \tag{7}$$

where $f(\eta)$ and $g(\eta)$ are the dimensionless stream functions, $f\theta(\eta)$ is the dimensionless temperature and primes denote differentiation with respect to η. Equation (1) is identically satisfied. By substituting (6) into Eqs. (2)–(5), the following ordinary differential equations will be obtained

$$f''' + (f+g)f'' + 1 - f'^2 = 0 \tag{8}$$

$$g''' + (f+g)g'' + 1 - g'^2 = 0 \tag{9}$$

$$\frac{1}{\mathrm{Pr}}\theta'' + (f+g)\theta' + Q\theta = 0 \tag{10}$$

and the boundary conditions become

$$f(0) = \gamma, \quad g(0) = 0, \quad f'(0) = \varepsilon_1, \quad g'(0) = \varepsilon_2, \quad \theta(0) = 1,$$
$$f'(\eta) \to 1, \quad g'(\eta) \to 1, \quad \theta(\eta) \to 0, \tag{11}$$

where $\mathrm{Pr} = \frac{\nu}{\alpha}$ is the Prandtl number, $Q = \frac{Q_0}{\rho C_p a}$ is the heat source parameter, $\gamma = -\frac{w_0}{\sqrt{a\nu}}$, $\gamma > 0$ indicates suction and $\gamma < 0$ corresponds to injection case, $\varepsilon_1, \varepsilon_2$ represents the stretching/shrinking parameter with $\varepsilon_1, \varepsilon_2 > 0$ for a stretching sheet and $\varepsilon_1, \varepsilon_2 < 0$ for a shrinking sheet, respectively.

The physical quantities of interest are the skin friction coefficient C_{fx} and C_{fy}, and the local Nusselt number, Nu_x which can be defined as

$$C_{fx} = \frac{\tau_{wx}}{\rho u_e^2}, \quad C_{fy} = \frac{\tau_{wy}}{\rho u_e^2}, \quad \mathrm{Nu}_x = \frac{x q_w}{k(T_w - T_\infty)}, \tag{12}$$

where τ_{wx} and τ_{wy} is the skin friction or wall shear stress along the x and y directions and q_w is the heat flux from the plate, which is given by

$$\tau_{wx} = \mu\left(\frac{\partial u}{\partial z}\right)_{z=0}, \quad \tau_{wy} = \mu\left(\frac{\partial v}{\partial z}\right)_{z=0}, \quad q_w = -k\left(\frac{\partial T}{\partial y}\right)_{z=0} \tag{13}$$

with μ and k is the dynamic viscosity and the thermal conductivity, respectively. Substituting (6) into (12) and using (11), the following expression can be obtained:

$$\mathrm{Re}_x^{\frac{1}{2}} C_{fx} = f''(0), \quad \mathrm{Re}_y x^{\frac{1}{2}} C_{fy} = g''(0), \quad \mathrm{Re}_x^{-\frac{1}{2}} \mathrm{Nu}_x = -\theta'(0), \tag{14}$$

where $\mathrm{Re}_x = \frac{u_e x}{\nu}$ and $\mathrm{Re}_y = \frac{u_e y}{\nu}$ is the local Reynolds numbers.

3. Stability analysis

In this section, we are concern about the unsteady state since the present study is capable of generating dual solutions that satisfy the corresponding boundary conditions. The stability analysis is performed by following the works done by Merkin [19], Weidman et al. [20], and Rosca and Pop [21]. Stability analysis is done by introducing the dimensionless time variable to clarify which solution is able to overcome the disturbance that been given to the flow which simply known as stable solution, while the solutions that promote the growth of the disturbance, known as unstable solution. Since the governing equations of the boundary layer problem which have been discussed in the basic equation section did not consider the time variable, thus, new governing equations of the unsteady-state problem is given by

$$\frac{\partial u}{\partial t} + u\frac{\partial u}{\partial x} + v\frac{\partial v}{\partial y} + w\frac{\partial w}{\partial z} = u_e\frac{du_e}{\partial x} + \nu\frac{\partial^2 u}{\partial z^2}, \tag{15}$$

$$\frac{\partial v}{\partial t} + u\frac{\partial v}{\partial x} + v\frac{\partial v}{\partial y} + w\frac{\partial v}{\partial z} = v_e\frac{dv_e}{\partial y} + \nu\frac{\partial^2 v}{\partial z^2}, \tag{16}$$

$$\frac{\partial T}{\partial t}+u\frac{\partial T}{\partial x}+v\frac{\partial T}{\partial y}+w\frac{\partial T}{\partial z}=\alpha\frac{\partial^2 T}{\partial z^2}+\frac{Q_0}{\rho C_p}(T-T_\infty), \tag{17}$$

where t denotes the time. The new similarity transformation of the unsteady-state problem by considering dimensionless time variable τ is introduced as

$$u=ax\frac{\partial f}{\partial \eta}(\eta,\tau),\quad v=ay\frac{\partial g}{\partial \eta}(\eta,\tau),\quad w=-\sqrt{a\nu}f(\eta,\tau)+g(\eta,\tau),$$

$$\eta=\sqrt{\frac{a}{\nu}}z,\quad \theta(\eta,\tau)=\frac{(T-T_\infty)}{(T_w-T_\infty)},\quad \tau=at. \tag{18}$$

Using (18) into Eqs. (15)–(17), the following equations are obtained:

$$\frac{\partial^3 f}{\partial \eta^3}+(f+g)\frac{\partial^2 f}{\partial \eta^2}-\left(\frac{\partial f}{\partial \eta}\right)^2+1-\frac{\partial^2 f}{\partial \eta\partial \tau}=0, \tag{19}$$

$$\frac{\partial^3 g}{\partial \eta^3}+(f+g)\frac{\partial^2 g}{\partial \eta^2}-\left(\frac{\partial g}{\partial \eta}\right)^2+1-\frac{\partial^2 g}{\partial \eta\partial \tau}=0, \tag{20}$$

$$\frac{1}{\mathrm{Pr}}\frac{\partial^2 \theta}{\partial \eta^2}+(f+g)\frac{\partial \theta}{\partial \eta}\theta'+Q\theta-\frac{\partial \theta}{\partial \tau}=0, \tag{21}$$

and the boundary conditions are as follows:

$$f(0,\tau)=\gamma,\quad g(0,\tau)=0,\quad \frac{\partial f}{\partial \eta}(0,\tau)=\varepsilon_1,\quad \frac{\partial g}{\partial \eta}(0,\tau)=\varepsilon_2,\quad \theta(0,\tau)=1,$$

$$\frac{\partial f}{\partial \eta}(\infty,\tau)\to 1,\quad \frac{\partial g}{\partial \eta}(\infty,\tau)\to 1,\quad \theta(\infty,\tau)\to 0. \tag{22}$$

Following Weidman et al. [20], to determine the stability of $f(\eta)=f(\eta_0)$, $g(\eta)=g(\eta_0)$, as well as $\theta(\eta)=\theta(\eta_0)$, which satisfy Eqs. (8)–(10) subject to the boundary conditions (10), let us write

$$f(\eta,\tau)=f_0+e^{-\lambda\tau}F(\eta,\tau), \tag{23}$$

$$g(\eta,\tau)=g_0+e^{-\lambda\tau}G(\eta,\tau), \tag{24}$$

$$\theta(\eta,\tau)=\theta_0+e^{-\lambda\tau}H(\eta,\tau), \tag{25}$$

where λ is an unknown eigenvalue, and $F(\eta,\tau)$, $G(\eta,\tau)$ and $H(\eta,\tau)$ are small relative to $f_0(\eta)$, $g_0(\eta)$ and $\theta(\eta)$. Substituting (23) into Eqs. (19)–(21), we obtained the following equations:

$$\frac{\partial^3 F}{\partial \eta^3}+(f_0+g_0)\frac{\partial^2 F}{\partial \eta^2}+(F+G)f_0''-(2f_0'-\lambda)\frac{\partial F}{\partial \eta}-\frac{\partial^2 F}{\partial \eta\partial \tau}=0, \tag{26}$$

$$\frac{\partial^3 G}{\partial \eta^3}+(f_0+g_0)\frac{\partial^2 G}{\partial \eta^2}+(F+G)g_0''-(2g_0'-\lambda)\frac{\partial G}{\partial \eta}-\frac{\partial^2 G}{\partial \eta\partial \tau}=0, \tag{27}$$

$$\frac{1}{\mathrm{Pr}}\frac{\partial^2 H}{\partial \eta^2}+(f_0+g_0)\frac{\partial H}{\partial \eta}+(F+G)\theta'+(Q+\lambda)H-\frac{\partial H}{\partial \tau}=0, \tag{28}$$

and the boundary conditions are as follows:

$$F(0,\tau)=0,\quad G(0,\tau)=0,\quad \frac{\partial F}{\partial \eta}(0,\tau)=0,\quad \frac{\partial G}{\partial \eta}(0,\tau)=0,\quad H(0,\tau)=1,$$

$$F'(\infty,\tau)=0,\quad G'(\infty,\tau)=0,\quad H(\infty,\tau)=0. \tag{29}$$

The solutions $f(\eta)=f(\eta_0)$, $g(\eta)=g(\eta_0)$, and $\theta(\eta)=\theta(\eta_0)$ of the steady Eqs. (8)–(10) are obtained by setting $\tau=0$. Hence, $F(\eta,\tau)$, $G(\eta,\tau)$ and $H(\eta,\tau)$ in (23)–(25) become

$$F'''+(f_0+g_0)F''+(F+G)f_0''-(2f_0'-\lambda)F'=0, \tag{30}$$

$$G'''+(f_0+g_0)G''+(F+G)g_0''-(2g_0'-\lambda)G=0, \tag{31}$$

$$\frac{1}{\mathrm{Pr}}H''+(f_0+g_0)H'+(F+G)\theta'+(Q+\lambda)H=0, \tag{32}$$

and the boundary conditions are as follows:

$$F(0) = 0, \quad G(0) = 0, \quad F'(0) = 0, \quad G'(0) = 0, \quad H(0) = 0,$$
$$F'(\eta) =\to 0, \quad G'(\eta) =\to 0, \quad H(\eta) =\to 0, \quad \text{as} \quad \eta \to \infty. \tag{33}$$

It should be mentioned that for particular values of Pr, Q, γ, ε_1 and ε_2, the stability of the corresponding steady flow solution $f(\eta) = f(\eta_0)$, $g(\eta) = g(\eta_0)$, and $\theta(\eta) = \theta(\eta_0)$ is determined by the smallest eigenvalue λ.

4. Results and discussion

The ordinary differential Eqs. (8)–(10) with the boundary conditions (11) were solved numerically using the bvp4c function in Matlab software. The numerical results obtained in terms of the skin friction coefficient, $\mathrm{Re}_x^{\frac{1}{2}} C_{fx}$, $\mathrm{Re}_y x^{\frac{1}{2}} C_{fy}$ the local Nusselt number, $\mathrm{Re}_x^{-\frac{1}{2}} \mathrm{Nu}_x$, velocity profile, $f'(\eta)$, $g'(\eta)$ and temperature profile, $\theta(\eta)$ for different values of suction/injection parameter, γ and heat source/sink parameter, Q, while the Prandtl number Pr is fixed at $\mathrm{Pr} = 1$ for the sake of brevity.

Table 1 shows that the present results match well with the previous results obtained by Wang [22] and Hafidzuddin et al. [6]. Table 1 clearly shows the values of skin friction coefficient $f''(0)$ for the case of stretching/shrinking sheet without heat source/sink effects $Q = 0$ (in Eq. (10)) and suction/injection effects $\gamma = 0$, in the boundary conditions (11). The comparisons shows that the present results match well with the previous results obtained by Wang [22] and Hafidzuddin et al. [6], and hence proves that the bvp4c program is a precise approach in solving the system numerically.

Table 1. Comparison of the values $f''(0)$ with those of Wang [22] and Hafidzuddin et al. [6] neglecting heat source/sink effect ($Q = 0$) in Eq. (10) and suction/injection effect ($\gamma = 0$) in the boundary conditions (11) for both stretching/shrinking sheet.

$f''(0)$						
	Wang [22]		Hafidzuddin et al. [6]		Present results	
$\varepsilon_1, \varepsilon_2$	First solution	Second solution	First solution	Second solution	First solution	Second solution
2.0					-2.131067	
1.5					-0.980173	
1.0					0	
0.5					0.780326	
0	1.311938		1.311938		1.311938	
-0.5					1.490011	
-1.0					1.161516	

Table 2. Smallest eigenvalue, λ for some values of ε_1 when $\mathrm{Pr} = Q = \gamma = 1$ and $\varepsilon_2 = -0.5$.

ε_1	First solution, λ	Second solution, λ
1	6.4283	-2.5496
0.5	6.0168	-1.6181
0	5.5520	-1.2567
-1	3.4316	-0.9839
-2	0.2610	-0.7142

The present study is able to produce more than one solution (dual solutions). Based on Figures 2, 4, 6 and 8, the dual solutions exist for both stretching/shrinking sheet which represents the variation of the skin friction coefficient $\mathrm{Re}_x^{\frac{1}{2}} C_{fx}$, $\mathrm{Re}_y x^{\frac{1}{2}} C_{fy}$ the local Nusselt number, $\mathrm{Re}_x^{-\frac{1}{2}} \mathrm{Nu}_x$, with the stretching/shrinking parameter ε_1 of x-direction for some values of γ and Q. Thus, the stability analysis has to be conducted to verify which solution is stable and physically reliable, by solving the eigenvalue problems in Eqs. (30)–(32) with boundary conditions (33). Table 2 shows the results from the stability analysis reveals that the first solution is stable because they attain positive smallest eigenvalues, while the second solutions are identified as unstable solutions and may not be realistic due to the negative smallest eigenvalues.

Figures 2, 4 and 6 show the variations of skin friction coefficient $\mathrm{Re}_x^{\frac{1}{2}} C_{fx}$, $\mathrm{Re}_y x^{\frac{1}{2}} C_{fy}$ the local Nusselt number, $\mathrm{Re}_x^{-\frac{1}{2}} \mathrm{Nu}_x$, respectively, for different values of suction/injection parameter γ. It can be seen from these Figures 2, 4 and 6, there are dual solutions exist for each value of γ under the

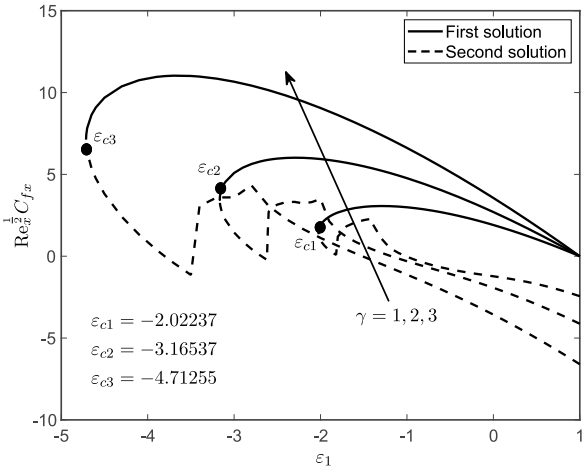

Fig. 2. Variation of the skin friction coefficient $\mathrm{Re}_x^{\frac{1}{2}} C_{fx}$, $\mathrm{Re}_y x^{\frac{1}{2}} C_{fy}$ with ε_1 for different values of γ when $\mathrm{Pr} = 1$, $Q = 1$, and $\varepsilon_2 = -0.5$.

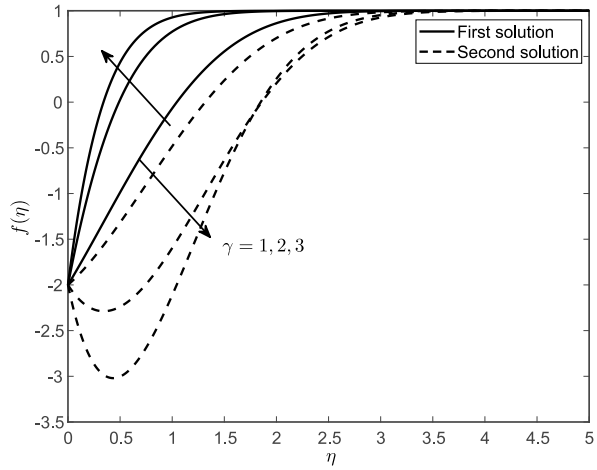

Fig. 3. The velocity profiles $f'(\eta)$ for different values of γ when $\mathrm{Pr} = 1$, $Q = 1$, $\varepsilon_2 = -0.5$ and $\varepsilon_2 = -2$ (shrinking case).

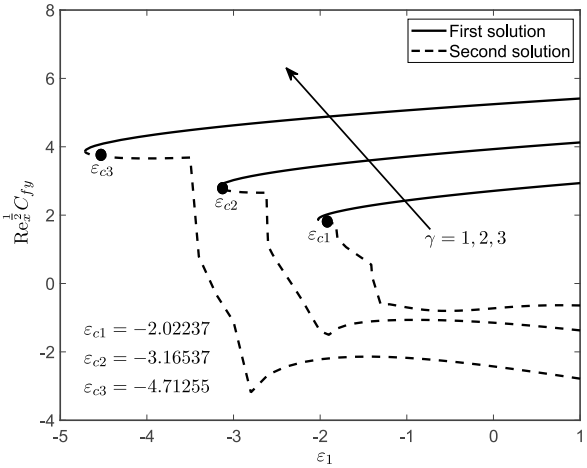

Fig. 4. Variation of the skin friction coefficient $\mathrm{Re}_x^{\frac{1}{2}} C_{fy}$, $\mathrm{Re}_y x^{\frac{1}{2}} C_{fy}$ with ε_1 for different values of γ when $\mathrm{Pr} = 1$, $Q = 1$, and $\varepsilon_2 = -0.5$.

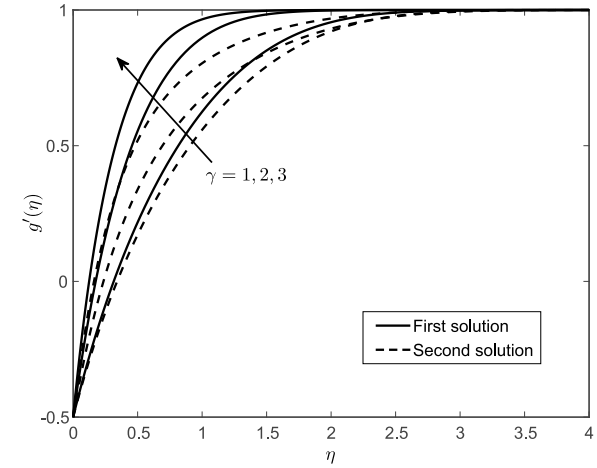

Fig. 5. The velocity profiles $g'(\eta)$ for different values of γ when $\mathrm{Pr} = 1$, $Q = 1$, $\varepsilon_2 = -0.5$ and $\varepsilon_2 = -2$ (shrinking case).

same value of stretching/shrinking parameter for ε_1 and ε_2. Dual solutions are obtained when $\varepsilon_1 > \varepsilon_2$ and no solutions obtained for $\varepsilon_1 < \varepsilon_2$, where ε_c is the critical values of ε_1, for which Eqs. (8)–(10) have no solutions and the full Navier–Stokes and energy equations should be solved. Based on our computation, the critical values ε_c obtained for $\gamma = 1$, 2 and 3 are $\varepsilon_{c1} = -2.02237$, $\varepsilon_{c2} = -3.16537$ and $\varepsilon_{c3} = -4.71255$ as shown in Figures 2, 4 and 6. The transition from positive (stable) to negative (unstable) values of γ occurs at the turning points, ε_c of the parametric solution curves ($\gamma = 1$, 2, 3) which is shown in Figures 2, 4 and 6.

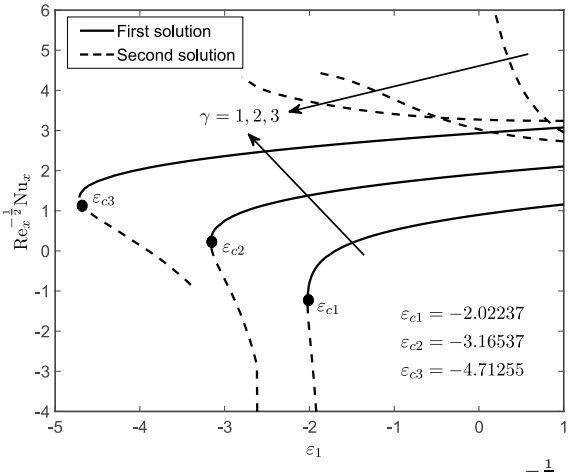

Fig. 6. Variation of the local Nusselt number $\mathrm{Re}_x^{-\frac{1}{2}} \mathrm{Nu}_x$ with ε_1 for different values of γ when $\mathrm{Pr} = 1$, $Q = 1$, and $\varepsilon_2 = -0.5$.

As shown in Figure 2, an upsurge in γ increases the skin friction coefficient of x-direction, $\mathrm{Re}_x^{\frac{1}{2}} C_{fx}$. Suction effect has the ability to reduce the thickness of the boundary layer thickness

which is reflected in Figure 3. These eventually will force the fluid flow to move slow and thus, increase the velocity gradient at the surface which is consistent with the graph in Figure 3. From Figure 2 also, it can be observed that the critical values stretching/shrinking parameter ε_c for which the solution exist increase as γ increases, suggests that suction widens the range of the dual solutions of the similarity Eqs. (8)–(10). Figure 3 depicts the velocity profile $f'(\eta)$ for different values of suction/injection parameter. For the stable solution, it is clearly indicate that the velocity is increased with an increase in the values of γ, whereas the second solution suggest otherwise. Physically, higher values of suction affect the fluid's velocity and reduce the friction losses and subsequently decrease the boundary layer thickness. The same trend occurs on the skin friction coefficient in y-direction $\mathrm{Re}_y x^{\frac{1}{2}} C_{fy}$ and velocity profile $g'(\eta)$ in Figures 4 and 5, respectively.

Figure 6 shows the influence of suction parameter on the local Nusselt number which represents the heat transfer rate. The local Nusselt number tends to increases as γ increases. The effect of suction will lower the thermal boundary layer thickness and it is clearly shown in Figure 7 which represents the temperature profile $\theta(\eta)$. Practically, suction is imposed in the system to enhance the competency of the diffusion process. As more heat is removed, the temperature is decreasing and the rate of heat transfer is getting higher.

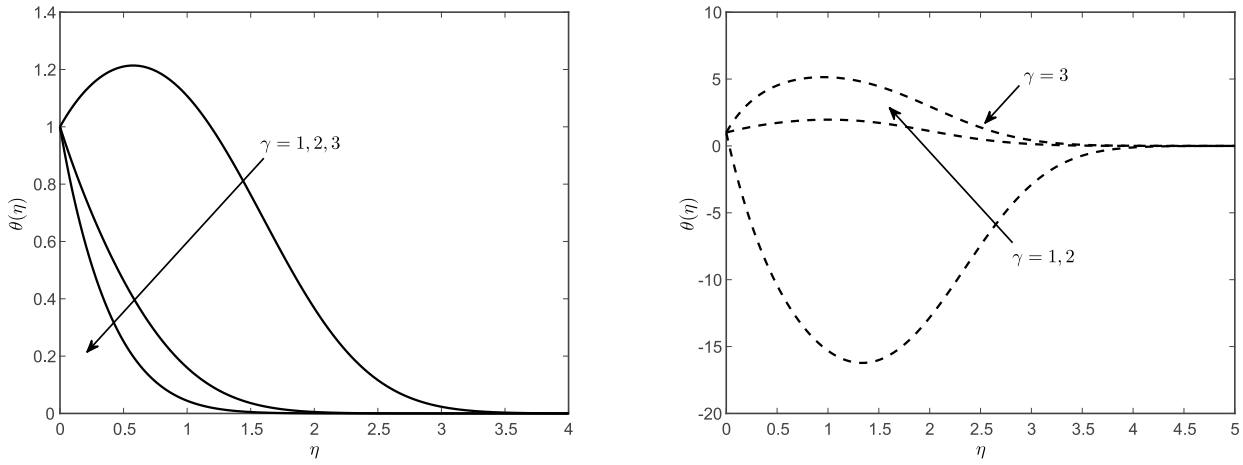

Fig. 7. The temperature profiles $\theta(\eta)$ First solution (right figure) and Second solution (left figure) for different values of γ when $\mathrm{Pr} = 1$, $Q = 1$, $\varepsilon_2 = -0.5$ and $\varepsilon_1 = -2$ (shrinking case).

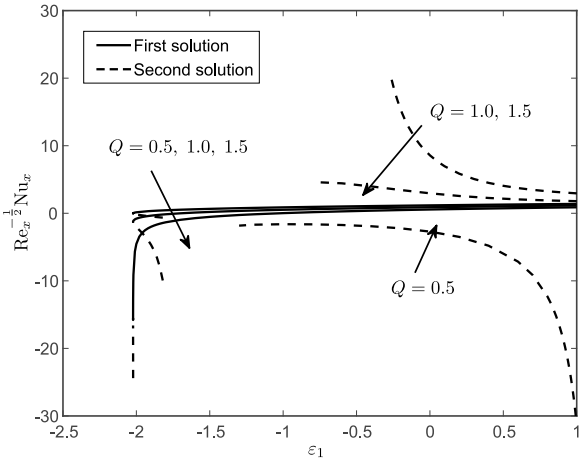

Fig. 8. Variation of the local Nusselt number $\mathrm{Re}_x^{-\frac{1}{2}}\mathrm{Nu}_x$ with ε_1 for different Q values of when $\mathrm{Pr} = 1$, $\gamma = 1$, and $\varepsilon_2 = -0.5$.

Figure 8 suggests that the local Nusselt number decrease as heat source parameter Q rises. Physically, heat source act like a heat generator, which releases the heat energy flow and enhanced the temperature profile $\theta(\eta)$ as depicted in Figure 9. From Figure 9, it is noticed that the thermal boundary layer thickness increase, so that increase the temperature gradient and in consequences the heat transfer rate at the surface is enhanced, which is consistent with the graph in Figure 8.

The velocity and temperature profiles which have been shown in Figures 3, 5, 7 and 9 satisfy the far field boundary conditions (11) asymptotically, which support the validity of the numerical results obtained and the existence of the dual solutions.

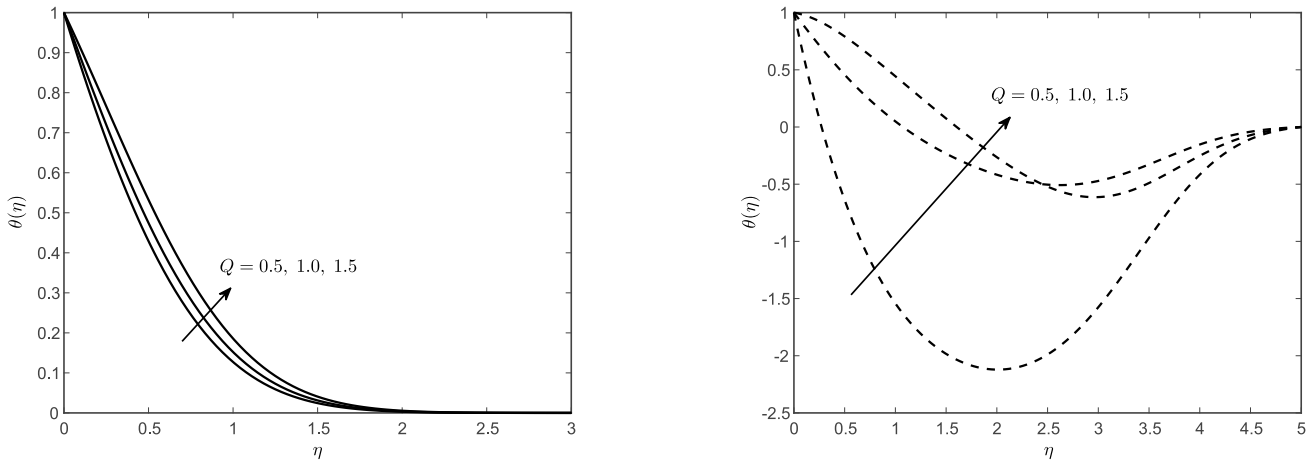

Fig. 9. The temperature profiles $\theta(\eta)$ first solution (right figure) and second solution (left figure) for different values of Q when $\mathrm{Pr} = 1$, $\gamma = 1$, $\varepsilon_2 = -0.5$ and $\varepsilon_1 = -2$ (shrinking case).

5. Conclusion

This paper explores the influence of suction and heat source parameters towards the three-dimensional stagnation point flow and heat transfer towards a permeable stretching/shrinking sheet. This problem was solved numerically using bvp4c function built in Matlab software. The analysis shows that the skin friction coefficient of x- and y-directions and the local Nusselt number as well as the velocity and temperature were influenced by suction/injection parameter. As the suction suction/injection increases, the skin friction coefficient of x- and y-directions and the local Nusselt number also increase. The rate of heat transfer decreases when the heat source parameter increases. Dual solution had been discovered for both stretching/shrinking sheet. Therefore, the stability analysis has been conducted to show the first solution is stable and physically reliable whereas the second solution is unstable.

[1] Hiemenz K. Die Grenzschicht an einem in den gleichformigen Flussigkeitsstrom eingetauchten geraden Kreiszlynder. Dingler's Polytechnical Journal. **326**, 321–340 (1911).

[2] Farooq U., Xu H. Free convection nanofluid flow in the stagnation-point region of a three dimensional body. The Scientific World Journal. **2014**, 158269 (2014).

[3] Kumar P., Prashu Nandkeolyar R. Modeling the hydromagnetic transient three-dimensional stagnation point flow of a couple stress Casson fluid over a bi-directional stretching sheet. Numerical Heat Transfer, Part B: Fundamentals. 1–19 (2024).

[4] Wahid N. S., Mustafa M. S., Arifin N. R., Pop I., Anuar N. S., Khashi'ie N. S. Numerical and statistical analyses of three-dimensional non-axisymmetric Homann's stagnation-point flow of nanofluids over a shrinking surface. Chinese Journal of Physics. **89**, 1555–1570 (2024).

[5] Shafie S., Kamal M. H. A., Jiann L. Y. N. A., Rawi N. A., Ali A. Quadratic Convective Nanofluid Flow at a Three-Dimensional Stagnation Point with the g-Jitter Effect. Journal of Advanced Research in Fluid Mechanics and Thermal Sciences. **93** (2), 111–124 (2022).

[6] Hafidzuddin E. H., Nazar R., Arifin N. M., Pop I. Effects of anisotropic slip on three-dimensional stagnation-point flow past a permeable moving surface. European Journal of Mechanics – B/Fluids. **65**, 515–521 (2017).

[7] Jamaludin A., Nazar R., Pop I. Three-dimensional mixed convection stagnation-point flow over a permeable vertical stretching/shrinking surface with a velocity slip. Chinese Journal of Physics. **55** (5), 1865–1882 (2017).

[8] Rehman F. U., Nadeem S., Haq R. U. Heat transfer analysis for three-dimensional stagnation-point flow over an exponentially stretching surface. Chinese Journal of Physics. **55** (4), 1552–1560 (2017).

[9] Al-Balushi L. M., Rahman M. M., Pop I. Three-dimensional axisymmetric stagnation-point flow and heat transfer in a nanofluid with anisotropic slip over a striated surface in the presence of various thermal conditions and nanoparticle volume fractions. Thermal Science and Engineering Progress. **2**, 26–42 (2017).

[10] Amirsom N. A., Uddin M. J., Ismail A. I. Three dimensional stagnation point flow of bionanofluid with variable transport properties. Alexandria Engineering Journal. **55** (3), 1983–1993 (2016).

[11] Bariş S., Dokuz M. S. Three-dimensional stagnation point flow of a second grade fluid towards a moving plate. International Journal of Engineering Science. **44** (1–2), 49–58 (2006).

[12] Mohaghegh M. R., Rahimi A. B. Three-dimensional stagnation-point flow and heat transfer of a dusty fluid toward a stretching sheet. Journal of Heat and Mass Transfer. **138** (11), 112001 (2016).

[13] Rehman F. U., Nadeem S., Rehman H. U., Haq R. U. Thermophysical analysis for three-dimensional MHD stagnation-point flow of nano-material influenced by an exponential stretching surface. Results in Physics. **8**, 316–323 (2018).

[14] Raju C. S. K., Sandeep N. Unsteady three-dimensional flow of Casson–Carreau fluids past a stretching surface. Alexandria Engineering Journal. **55** (2), 1115–1126 (2016).

[15] Hayat T., Shehzad S. A., Alsaedi A. Three-Dimensional Flow of Jeffrey Fluid over a Bidirectional Stretching Surface with Heat Source/Sink. Journal of Aerospace Engineering. **27** (4), 4014007 (2014).

[16] Hayat T., Alsaedi A. Soret and Dufour effects in three-dimensional flow over an exponentially stretching surface with porous medium, chemical reaction and heat source/sink. International Journal of Numerical Methods for Heat & Fluid Flow. **25** (4), 762–781 (2015).

[17] Kar M., Dash G. C., Sahoo S. N., Rath P. K. Three-dimensional free convection MHD flow in a vertical channel through a porous medium with heat source and chemical reaction. Journal of Engineering Thermophysics. **22** (3), 203–215 (2013).

[18] Hafidzuddin M. E. H., Nazar R., Arifin N. M., Pop I. Three-dimensional viscous flow and heat transfer over a permeable shrinking sheet. International Communications in Heat and Mass Transfer. **56**, 109–113 (2014).

[19] Merkin J. H. On dual solutions occurring in mixed convection in a porous medium. Journal of Engineering Mathematics. **20**, 171–179 (1985).

[20] Weidman P. D., Kubitschek D. G., Davis A. M. J. The Effect of Transpiration on Self-Similar Boundary Layer Flow Over Moving. International Journal of Engineering Science. **44** (11–12), 730–737 (2006).

[21] Rosca N. C., Pop I. Mixed convection stagnation point flow past a vertical flat plate with a second order slip: Heat flux case. International Journal of Heat and Mass Transfer. **65**, 102–109 (2013).

[22] Wang C. Y. Stagnation slip flow and heat transfer on a moving plate. Chemical Engineering Science. **61** (23), 7668–7672 (2006).

Аналіз стійкості тривимірного потоку в точці застою та теплообміну через проникний лист, що розтягується/стискається, з ефектом джерела тепла у в'язкій рідині

Камал Ф.[1], Займі К.[1,2], Хамід Р. А.[1], Бакар Н. А. А.[1], Сайдін Н. А.[1], Халім А. А. А.[3]

[1] *Інститут інженерної математики, Малайзійський університет Перліс, Кампус Пау Путра, 02600 Арау, Перліс, Малайзія*
[2] *Центр передового досвіду соціальних інновацій та сталого розвитку (CoESIS), Малайзійський університет Перліс, Кампус Пау Путра, 02600 Арау, Перліс, Малайзія*
[3] *Факультет технологій електронної інженерії (FTKEN), Малайзійський університет Перліс, Кампус Пау Путра, 02600 Арау, Перліс, Малайзія*

У цій статті досліджується постійний тривимірний потік у точці застою до проникного листа, що розтягується/стискається, за наявності ефектів джерела тепла. Основні рівняння у формі диференціальних рівнянь у частинних похідних перетворюються на систему звичайних диференціальних рівнянь за допомогою перетворення подібності, а потім розв'язуються чисельно за допомогою функції bvp4c у програмному забезпеченні Matlab. Отримано різні чисельні розв'язки для коефіцієнта поверхневого тертя та локального числа Нуссельта, а також профілів швидкості та температури для кількох значень основних параметрів. Виявлено, що існують подвійні розв'язки для випадку розтягування/стискання. Здійснено аналіз стійкості, щоб визначити, який розв'язок є стійким і фізично реалізованим. Результати аналізу стійкості показують, що перший розв'язок є стійким, а другий — ні.

Ключові слова: *тривимірний потік; точка застою; ефект всмоктування/впорскування; ефект джерела тепла; лист, що розтягується/стискається; аналіз стійкості.*